

# RSC Advances



This is an *Accepted Manuscript*, which has been through the Royal Society of Chemistry peer review process and has been accepted for publication.

*Accepted Manuscripts* are published online shortly after acceptance, before technical editing, formatting and proof reading. Using this free service, authors can make their results available to the community, in citable form, before we publish the edited article. This *Accepted Manuscript* will be replaced by the edited, formatted and paginated article as soon as this is available.

You can find more information about *Accepted Manuscripts* in the [Information for Authors](#).

Please note that technical editing may introduce minor changes to the text and/or graphics, which may alter content. The journal's standard [Terms & Conditions](#) and the [Ethical guidelines](#) still apply. In no event shall the Royal Society of Chemistry be held responsible for any errors or omissions in this *Accepted Manuscript* or any consequences arising from the use of any information it contains.

## ARTICLE

## Fabrication of High Power $\text{LiNi}_{0.5}\text{Mn}_{1.5}\text{O}_4$ Battery Cathodes by Nanostructuring of Electrode Materials

Cite this: DOI: 10.1039/x0xx00000x

Mohammad Ali Kiani<sup>†,‡</sup>, Mohammad Safi Rahmanifar<sup>||</sup>, Maher F. El-Kady<sup>§,+</sup>, Richard B. Kaner<sup>§,\*</sup>, and Mir Fazlollah Mousavi<sup>‡,§,\*</sup>Received 00th January 2012,  
Accepted 00th January 2012

DOI: 10.1039/x0xx00000x

www.rsc.org/

Using nanoparticles, instead of microparticles, as active electrode materials in lithium ion batteries could provide a solution to slow charging rates due to long ion diffusion pathways in conventional bulk materials. In this work, we present a new strategy for the synthesis of high purity lithium nickel manganese oxide ( $\text{LiNi}_{0.5}\text{Mn}_{1.5}\text{O}_4$ ) nanoparticles as a high-voltage cathode. A sonochemical reaction is used to synthesize nickel hydroxide and manganese dioxide nanoparticles followed by a solid-state reaction with lithium hydroxide. The product shows a single spinel phase and uniform spherical nano-particles under the appropriate calcination conditions. The  $\text{LiNi}_{0.5}\text{Mn}_{1.5}\text{O}_4$  exhibits a high voltage plateau at about 4.7–4.9 V in the charge/discharge process and delivers a discharge capacity of more than 140 mAh g<sup>-1</sup> and excellent cycling performance with 99% capacity retention after 70 cycles. The synthesized nano-particles show improved electrochemical performance at high rates. This electrode delivers a power density as high as 26.1 kW kg<sup>-1</sup> at a discharge rate of 40 C. This power performance is about one order of magnitude higher than traditional lithium ion batteries. These findings may lead to a new generation of high power lithium ion batteries than can be recharged in minutes instead of hours.

### Introduction

Lithium-ion batteries have gained enormous interest recently for large-scale applications, such as electric vehicles, hybrid electric vehicles, and stationary energy storage<sup>1</sup>. To meet the requirements of these applications, further improvements in terms of energy and power density are required. The transition-metal-doped spinel-type  $\text{LiM}_x\text{Mn}_{2-x}\text{O}_4$  (where M is Ni<sup>2,3</sup>, Fe<sup>4</sup>, Cr<sup>5</sup>, Co<sup>6</sup>, etc.) offers cathode materials with one of the highest potentials for high power Li batteries. The voltage plateau and capacity in a  $\text{Li}/\text{LiM}_x\text{Mn}_{2-x}\text{O}_4$  cell strongly depend on the type of transition metal (M) and its constituents. The charge/discharge reaction mechanism is based on oxidation/reduction of the doped transition metal above 4.6 V. Among all possible compositions,  $\text{LiNi}_{0.5}\text{Mn}_{1.5}\text{O}_4$  (LNMO) is the most attractive since it offers a flat plateau at 4.7 V, due to the  $\text{Ni}^{2+}/\text{Ni}^{4+}$  couple, with a capacity of > 130 mAh g<sup>-1</sup>, and good cycling stability and rate capability<sup>8-22</sup>.

There are two possible lattice structures for LNMO depending on the Ni ordering in the lattice<sup>13,23</sup>. One is primitive simple cubic ( $P4_332$ ), and the other is face centered spinel ( $Fd3m$ ). The Structural differences between these two space groups are described in the supporting information.

To meet the high power demands of lithium ion batteries in new applications, the rate capability of LNMO needs to be significantly improved. To reach this goal, two methods can be

used: (1) increasing the electronic conductivity by controlling of the electrode microstructure, or (2) enhancing the Li-ion transport by reducing the bulk diffusion length in the active phase, which can be achieved by the use of nanostructured materials. The relatively low conductivity is one of the main drawbacks of LNMO, restricting its high-rate performance. To enhance conductivity, nanosized LNMO materials have been synthesized by various methods to shorten the transport length of Li<sup>+</sup> ions and electrons, and improved high-rate performances have been achieved<sup>24-27</sup>. Different methods of synthesis can result in LNMO with different sizes, morphologies, crystal structures and electrochemical properties<sup>23,24,28-30</sup> (Table S2). Brutti and coworkers investigated various synthesis methods for the LNMO spinel including: wet chemistry, solid state reactions, combustion synthesis, cellulose-based sol-gel synthesis, ascorbic acid-based sol-gel synthesis and resorcinol/formaldehyde-based sol-gel synthesis for applications as cathode materials in lithium ion batteries<sup>30</sup>. Most of these methods include two or more steps which involve the preparation of precursors at low temperatures followed by heating at high temperatures to obtain LNMO. However, the

use of expensive raw materials and the presence of impurities and aggregations in the products remain challenging.

Nanostructured materials can provide new solutions for a variety of applications<sup>31</sup> For example, our research group has used nanomaterials to enable a new generation of batteries<sup>32-35</sup>, supercapacitors<sup>36-41</sup>, sensors<sup>42-45</sup> and solid phase microextraction systems<sup>46</sup>. In this work, we show that by engineering the structure of LNMO at the nanoscale, it is possible to fabricate high power lithium batteries that can be charge/discharged at high rates up to 40C (where 1C rate represents a one-hour complete charge or discharge). A single phase LNMO product with space group  $P4_332$  that did not contain nickel oxide impurities was obtained with the appropriate synthesis conditions, i.e. calcination temperature and time, were employed. These electrodes demonstrate stable and highly reversible capacity of about 141 mAh/g while providing higher voltage than the traditional manganese-only  $\text{LiMn}_2\text{O}_4$  electrodes. In addition, this nano-sized and ordered LNMO offers high rate performance, flat voltage plateau and good cycling stability, which is an important step towards the successful utilization of high-voltage spinels for the next generation lithium ion batteries.

## Experimental Section

### Aparatus

A multiwave ultrasonic generator (Sonicator® 3000; Misonix, Inc., Farmingdale, NY, USA), equipped with a converter/transducer and titanium oscillator (horn), 12.5 mm in diameter, operating at 20 kHz with a maximum power output of 600 W, was used for the ultrasonic irradiation. The ultrasonic generator automatically adjusted the power level. The wave amplitude in each experiment was adjusted as needed. A cylindrical two-walled glass cell with an interior volume of 300 mL was used for the sonication of the reaction solution. The solution temperature was kept constant by circulating water from a water bath (Optima, Tokyo, Japan). A home-made centrifuge, with a maximum speed of 8000 rpm, was used for the deposition of the dispersed nano-particles. For milling precursors, a Retsch mixer/mill (RM 100) was employed. An electrical furnace (Paragon E10, USA) was used to heat the samples. X-ray diffraction ( $\text{Cu K}\alpha$ ,  $\lambda = 1.5406 \text{ \AA}$ ) (Philips X'pert diffractometer), scanning electron microscopy (SEM) (Philips XL 30) were used to characterize the as-prepared powders. The cyclic voltammetry (CV), electrochemical impedance spectroscopy (EIS) measurements were carried out using Galvanostat/PotentiostatAutolab (PGSTAT30) connected to a PC. Electrochemical charge/discharge experiments were performed on a Solartron SI 1470.

### Synthesis of nano-LNMO particles

Sonochemical synthesis of  $\text{Ni}(\text{OH})_2$  was carried out as previously reported<sup>32</sup>. Briefly, 100 mL of 0.1 M  $\text{NiCl}_2 \cdot 6\text{H}_2\text{O}$  and 0.8 mM CTAB were prepared and sonicated for 5 min in a sonication flask. Then, 100 mL of 0.2 M NaOH was added dropwise into the sonication flask over 45 min. The precipitate was allowed to settle for 2 h and the colloidal suspensions were centrifuged and washed with distilled water. The precipitate was dried to a constant weight (24 h) in an oven at 70 °C and characterized as  $\text{Ni}(\text{OH})_2$ . Nano-particles of  $\text{MnO}_2$  were prepared by an oxidation reaction under ultrasonication based on previous reports<sup>33, 35</sup>. Briefly, nano-particles of  $\gamma\text{-MnO}_2$  were synthesized by a redox reaction between stoichiometric quantities of  $\text{MnSO}_4 \cdot \text{H}_2\text{O}$  and  $(\text{NH}_4)_2\text{S}_2\text{O}_8$  in the presence of an ultrasonic wave.

LNMO nano-particles were synthesized using a stoichiometric amount of  $\text{LiOH}$ , nano- $\text{Ni}(\text{OH})_2$ , and nano- $\text{MnO}_2$  (2.12:1:3) which were thoroughly mixed using a Retsch mixer/mill for 1 h. Next, the mixtures were calcined at 800 °C for 24 h, and subsequently cooled to room temperature. The resulting powders were thoroughly washed several times with distilled water, centrifuged and dried for 24 h in oven at 100 °C. Scheme S1 shows a schematic representation of the preparation of the  $\text{LiNi}_{0.5}\text{Mn}_{1.5}\text{O}_4$  nanostructures.

### Electrochemical investigations

The electrochemical performances of the as-prepared powders were investigated with a beaker-type three-electrode cell. The working electrode was composed of 80% LNMO, 15% carbon (Merck) and 5% Teflon (polytetrafluoroethylene) (a 60% water-based solution from SUTTECH, Iran) binder by weight. This blend was rolled and pressed onto a nickel grid current collector, and the electrode was dried at 120 °C for 12 h in an oven. In a typical experiment, the active mass loading is between 8 and 9 mg. The three-electrode cell consisted of an LNMO working electrode and a pressed Li granule (Fluka) on a Ni grid current collector was used for the electrochemical measurements both as a counter and a reference electrode. The electrolyte was 1M  $\text{LiClO}_4$  (Acros) in propylene carbonate (PC) (Merck). The assembly of the cells was carried out in a dry Ar-filled glove box. CV and EIS experiments were done in three-electrode systems. The cyclic voltammogram was measured at a sweep rate of 0.1  $\text{mV s}^{-1}$  between 3.5 and 5.0 V. The EIS experiments were performed at different applied voltages (4.3-5.0 V) over a frequency range of 100 kHz to 10 mHz with a perturbation amplitude of 5 mV. EIS data analyses were carried out based on CNLS method of Boukamp using Zview2 software (Scribner Associates), with an appropriate equivalent circuit as described in the text. It should be noted that in all cases, the uncertainty in data fitting was approximately < 10%. Galvanostatic charge/discharge measurements were performed in a two-electrode system within a potential range of 4.5–5.0 V versus  $\text{Li/Li}^+$ . This electrochemical cell is composed of a LNMO cathode, 1M  $\text{LiClO}_4$  in PC as the electrolyte, and lithium metal as the anode. All the electrochemical tests were done at 2 °C.

## Result and Discussion

### Characterisation of LNMO

#### Crystal and morphological studies

The crystal structure of the LNMO particles was examined by XRD as shown in Fig. 1a. The pattern is typical of the spinel structure<sup>47</sup>, indicating no impurities present in the compound. This is very important because in synthesizing LNMO, impurities such as NiO and  $\text{Li}_x\text{Ni}_y\text{O}$  usually exist in the products, which can deteriorate their electrochemical performance<sup>48, 49</sup>. All these peaks indicate a primitive simple cubic structure (JCPDS#802184) with the space group  $P4_332$ <sup>50, 51</sup> (Fig. 1b). In this space group Li atoms are in 8c sites, Ni atoms in 4b sites, Mn atoms in 12d sites, and O atoms in 8c and 24(e) sites<sup>51, 52</sup>. As previously mentioned, the crystal structure has a significant effect on electrochemical properties. LNMO with the  $Fd3m$  space group has two distinct plateaus during the charge and discharge process around 4.7 V corresponding to the  $\text{Ni}^{2+/4+}$  redox couple<sup>53</sup>. For the  $P4_332$  space group, these two plateaus are not readily observed. Scanning electron microscopy (SEM) shows that the LNMO possesses uniform particles with semispherical-like shapes and a particles size is between 20 -50 nm, Fig. 1c. These

nanoparticles are composed of nondistinct grains with a rough surface and large porosity, which could facilitate the diffusion of electrolyte into the electrode materials during charge and discharge processes.

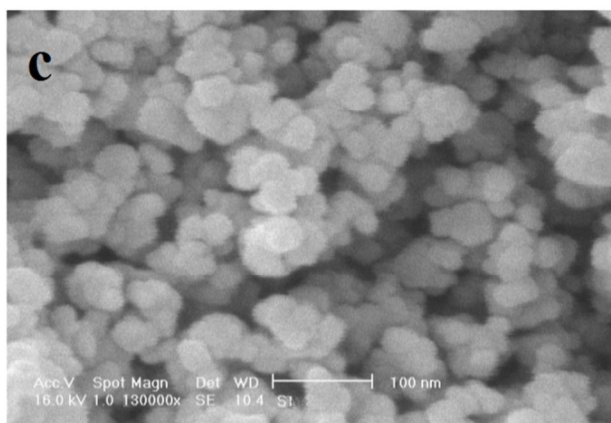
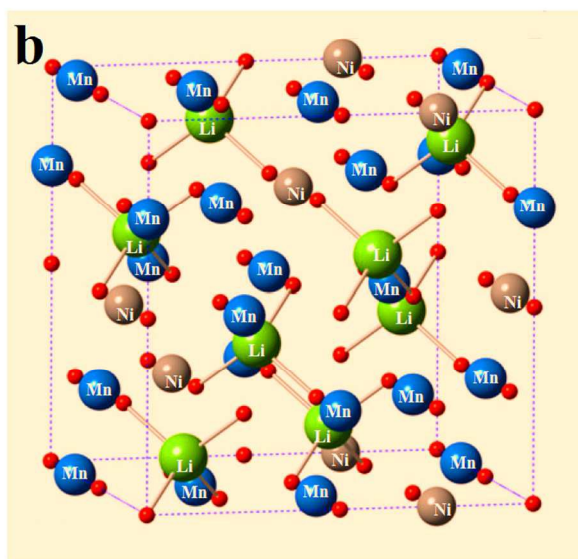
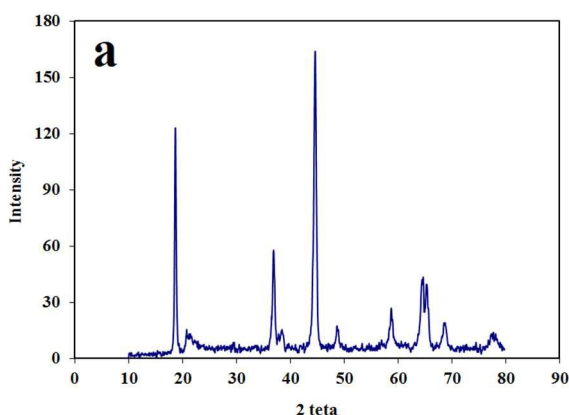


**Figure 1.** (a) X-ray diffraction patterns (b) LNMO with  $P4_332$  space group (c) Scanning electron micrographs of prepared LNMO.

### Electrochemical investigations

Figure 2a displays a cyclic voltammogram of a LNMO electrode at the scan rate of  $0.1 \text{ mV s}^{-1}$  in the voltage range of

3.5–5.0 V versus  $\text{Li/Li}^+$  in a 1 M  $\text{LiClO}_4$  in propylene carbonate electrolyte. Two resolved peaks at 4.72 (a1) and 4.78 V (a2) on the forward scan, and two peaks at 4.71 (c2) and 4.66 V (c1) on the reverse scan are observed. This operating potential is higher than the undoped spinel LMO ( $a1=3.95$ ,  $a2=4.18$ ,  $c1=3.92$ ,  $c2=4.15 \text{ V}$ )<sup>33</sup>, indicating the importance of  $\text{Ni}^{2+}$  ion doping. The higher potential of LNMO can be attributed to the removal of two electrons occupying the position of the  $\text{Ni}^{2+}$  3d  $e_g$  levels with respect to the  $\text{Mn}^{4+}$  3d  $e_g$  levels which no electrons. Accordingly, the  $e_g$  level of  $\text{Ni}^{2+}$  filled with two electrons is about 0.5 eV higher than the empty  $\text{Mn}^{4+}$   $e_g$  level, leading to an increase of the operating voltage<sup>54</sup>. The two sets of redox couples appearing in the CV profiles correspond to distinct redox voltages for  $\text{Ni}^{2+}/\text{Ni}^{3+}$  and  $\text{Ni}^{3+}/\text{Ni}^{4+}$  as reported by others<sup>55</sup>. The potential difference between the peaks in each of these redox couples are 0.06 and 0.07 V, which suggests the redox system is reversible. In LNMO,  $\text{Ni}^{2+}$  exists at the 16d site, instead of  $\text{Mn}^{3+}$ , and their redox reactions are related to the Li-ion extraction/insertion at 5 V<sup>4</sup>. For stoichiometric LNMO, all Ni exists in the 2+ oxidation state and all Mn exists in the 4+ oxidation state, resulting in the absence of the 4 V potential plateau<sup>33, 52</sup>. In other words, in LNMO nickel rather than manganese is involved in the electrochemical redox reactions.

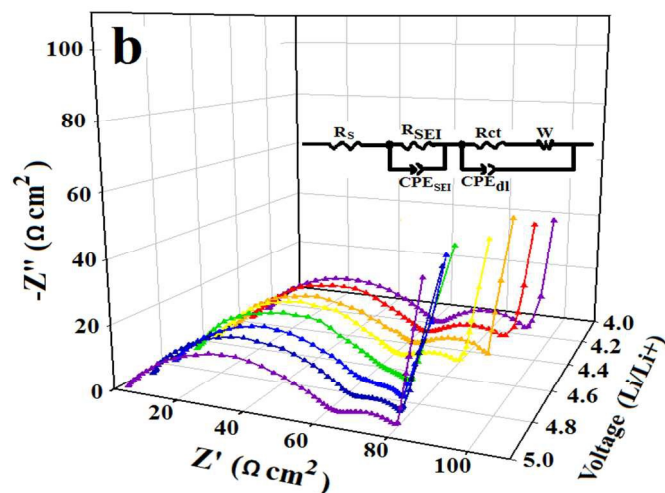
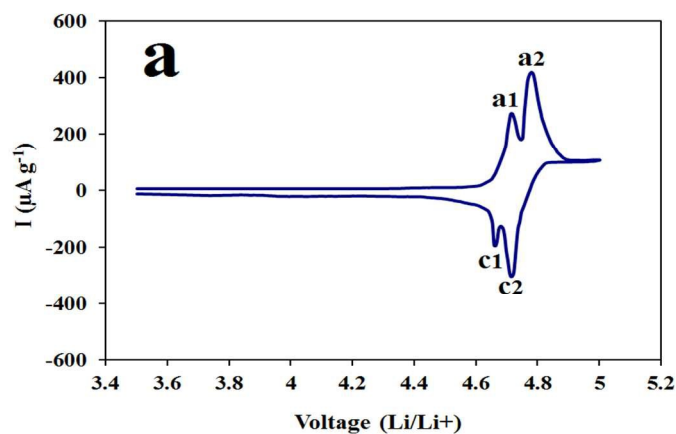


**Figure 2.** (a) Cyclic voltammogram of the LNMO at the scan rate of  $0.1 \text{ mV s}^{-1}$  in 1.0 M  $\text{LiClO}_4$  at  $25^\circ \text{C}$ . (b) Potential effect on Nyquist plots of LNMO nano-particles electrodes at different applied voltages (inset is its equivalent circuit).

The presence of manganese in the redox reactions increases the possibility of Jan–Teller distortion<sup>56</sup>, and may thus reduce the life cycle. The cathode showed very stable electrochemical performance without any noticeable degradation of the electrolyte solution in the operational potential range of this electrode during cycling test. Electrochemical impedance spectroscopy (EIS) could help provide an understanding of the electrochemical behavior of the LNMO electrodes. Figure 2b displays Nyquist plots of a LNMO electrode at different applied voltages (4.3–5.0 V). The applied voltage values were selected carefully to test the electrochemical behavior of the electrodes before and after the intercalation of lithium ions. As shown in Fig. 2b, all Nyquist spectra are comprised of a semicircle in the high frequency range, another semicircle in the medium-to-low frequency range and a sloping line at the low frequency range, being attributed to the resistance of Li<sup>+</sup> ion migration through the surface layer, charge transfer resistance, and diffusion of Li<sup>+</sup> in the solid electrode, respectively<sup>57,58</sup>. The impedance spectra can be explained on the basis of an equivalent circuit which is presented as an inset of Fig. 2b<sup>59</sup>. In this circuit, R<sub>S</sub> is the electrolyte resistance, R<sub>SEI</sub> is the solid electrolyte interface, R<sub>ct</sub> is the charge transfer resistance, W is the Warburg impedance, and CPE<sub>SEI</sub> and CPE<sub>di</sub> are constant phase elements. The solution resistance (R<sub>S</sub>) and solid electrolyte interface (R<sub>SEI</sub>) resistance changed only slightly because the electrolyte and the surface film were stable during cycling for the cell and they are nearly potential-independent<sup>60</sup>. In contrast to the resistance of the solid electrolyte interface, charge transfer resistance is largely potential-dependent. As can be seen from Fig. 2b, a significant change in the diameter of the second semicircle is observed by changing the applied potential, which mainly reflects the change of charge-transfer resistance.

The charge transfer resistance fitting results are summarized in Table S1. The charge transfer resistance decreased with increasing the electrode potential from 4.3 to 4.7 V, and then increased with increasing potential from 4.8 to 5.0 V. This result is consistent with the analysis in Fig. 2a. These results show that nanostructured LNMO spinel has faster Li-ion and electron transport at the interfaces between the electrolyte and the electrodes and shows its improved performance at higher voltage than nanostructured LMO which was previously reported by our group<sup>33</sup> (For LMO R<sub>ct</sub> = 10 Ω.cm<sup>2</sup> at operating voltage of 4.1 V and for LNMO R<sub>ct</sub> = 7 Ω.cm<sup>2</sup> at operating voltage of 4.7 V).

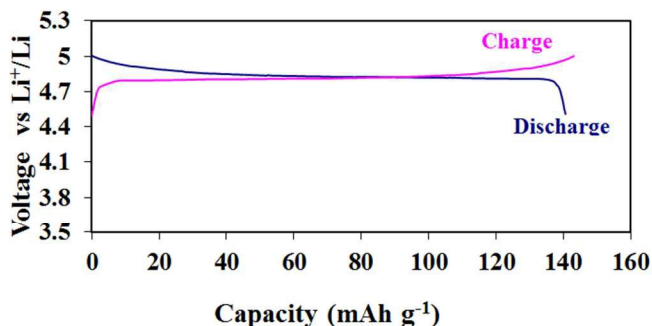


**Figure 3.** Charge/discharge of LNMO spinel with rate of 0.5 C in 1.0 M LiClO<sub>4</sub> at 25 °C.

The initial charge and discharge curves of LNMO are illustrated in Fig. 3. The charge curves exhibit a very flat voltage profile at around 4.7 V region, which is attributed to the oxidation of Ni<sup>2+</sup> first to Ni<sup>3+</sup> and Ni<sup>3+</sup> then to Ni<sup>4+</sup> during

charging<sup>61</sup>. In this study, the charge/discharge process was carried out over a narrow potential window of 0.5 V and this is where the specific capacities were calculated in this work, while the capacities reported in Table S2 are often the result of a larger potential range of 1.5 V. It has been previously demonstrated that LNMO with a disordered structure (*Fd3m*) shows two obvious voltage plateaus at around 4.7 V,<sup>3,52,62,63</sup> while that with an ordered structure (*P4<sub>3</sub>32*) gives a flat voltage profile at around 4.7 V<sup>51</sup>. Therefore, the observation of one distinct plateau at about 4.7 V, in Fig. 3 confirms the ordered structure of LNMO and is consistent with the XRD analysis. The initial specific charge and discharge capacities are 143.1 and 140.6 mAh g<sup>-1</sup>, respectively, and therefore the columbic efficiency is greater than 98%.

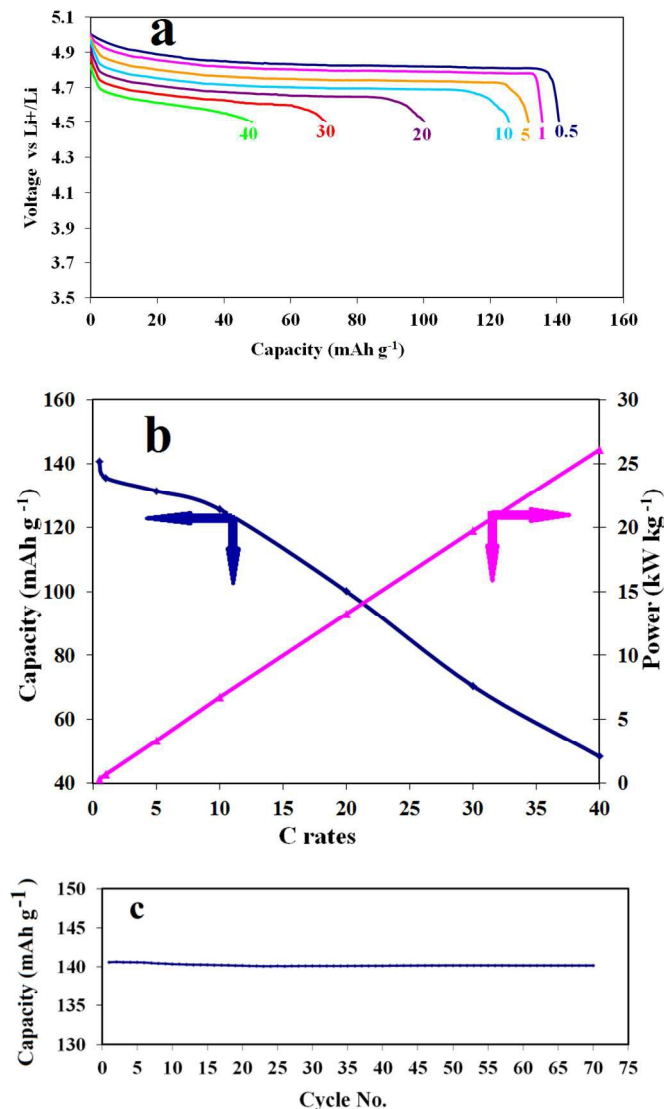


**Figure 4.** (a) Rate performance of the LNMO nano-particles (b) Specific capacity & power vs C rates. (c) Cyclic performance of the LNMO nano-particles at 0.5 C.

Because LNMO spinel is used primarily for high power applications, the rate of lithium intercalation–deintercalation is especially important. Figure 4a shows the electrode response at various C-rate currents. The charge current density was kept at a constant rate of 1 C, while the discharge currents were

changed from 0.5 C to 1, 5, 10, 20, 30 and 40 C in subsequent cycles. The discharge capacities and power densities at different C rates are shown in Fig 4b. The power densities were calculated from the following equation<sup>64</sup>:

$$P = i \times V_{mid} \quad (1)$$

Where  $i$  is discharge current density and  $V_{mid}$  is the midpoint voltage of the discharge plot. Figure 4b shows the excellent rate-capability of the electrode that can operate at a rate as high as 10 C, while still maintaining 89% of the 0.5 C discharge rate capacity. Although the capacity decay is faster at higher rates, it still delivers about 50% of its initial capacity even when fully discharged in 2 min (30 C rate). This rate performance compares with literature reports for ordered LNMO spinel. It should be mentioned here that the high rate performance reported in Ref.<sup>2</sup> was only obtained in the presence of a large amount of carbon (65 wt %). The spinel LNMO studied here can provide 26 kW kg<sup>-1</sup> based on the total mass of the active materials. Since active materials typically account for 30% of the mass of a fully packaged cell, the power density would be 7.8 kW kg<sup>-1</sup>. This power performance is higher than nickel metal-hydride (0.1-1 kW kg<sup>-1</sup>) and common lithium-ion batteries (0.8-2 kW kg<sup>-1</sup>)<sup>64</sup>. These findings indicate that the nanostructured LNMO cathode material can be used to build superior energy storage devices for HEVs and EVs offering both high-power and high-energy densities.

The excellent rate performance can be attributed to the ultrasonic cavitation that has a direct effect on the formation of the synthesized precursor. It could change the hydrolysis, condensation, nucleation and crystal growth processes<sup>65, 66</sup>. This may change the microstructure of the material and result in a more homogeneous distribution of elements in the lattice, which could in turn make full use of the charge-discharge reactions. Trivial size effects e.g. an increased surface-to-volume ratio and shorter length displacements for Li<sup>+</sup> ions<sup>24, 28, 67</sup> can also improve the rate capability and cycle life of cells<sup>68</sup>. Furthermore, the large surface area of the electrode and electrode/electrolyte interface provide additional advantages for LNMO nanoparticles such as (1) improved reaction kinetics that results in increased development and reversibility of the lithium insertion/extraction process, which improve cell capacity and capacity retention; and (2) the ability to use high charge/discharge rates.

Figure 4c shows the cycling performance of the LNMO electrode at 0.5 C. The LNMO electrode delivers an initial discharge capacity 140.6 mAh g<sup>-1</sup> and after 70 cycles the total discharge capacity is 140.1 mAh g<sup>-1</sup>, demonstrating a capacity retention > 99%. We attribute this excellent cycling performance to the existence of Mn<sup>4+</sup> alone and no impurity phases resulting from Li, Ni, and Mn atoms that are rather uniformly distributed on the atomic scale. This is also consistent with recent studies showing that unlike disordered materials, nanoscaling of ordered structures can be an effective strategy for not only higher rate capability but also better stability<sup>14-16, 69</sup>.

A Ragone plot showing the energy density and power density of LNMO-based lithium ion batteries calculated based on the active mass of the electrode materials is presented in Fig. 5. As can be seen this battery can provide much higher energy density compared to conventional rechargeable batteries such as Li ion and nickel-metal hydride batteries.

## Conclusions

LiNi<sub>0.5</sub>Mn<sub>1.5</sub>O<sub>4</sub> nanoparticles with high homogeneity, spherical morphology, and cubic structure with space group  $P4_332$  have been prepared by two-step method: 1. sonochemical and 2. solid state reaction. The CV results showed two pair of reversible peaks at about 4.7 V. The synthesized product as a cathode material has an excellent charge and discharge efficiency. This

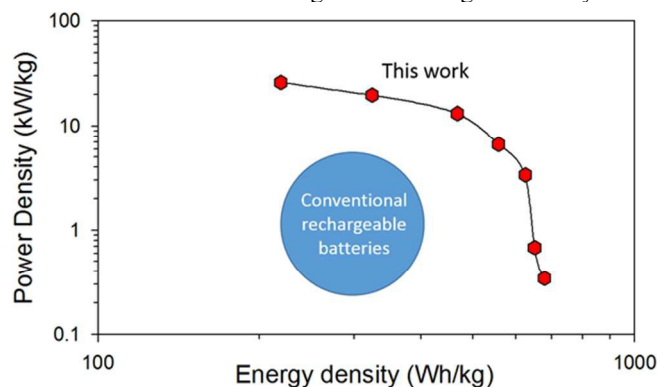


Figure 5. Ragone plot for synthesized LNMO.

material has the ability to discharge at high rate and high power, even up to 40 C and 26.1 kW kg<sup>-1</sup>, respectively. The LNMO nanoparticle cathode showed excellent cycle performance between 4.5 and 5.0 V, exhibiting a stable and highly reversible capacity of about 141 mAh g<sup>-1</sup> for 70 cycles. These excellent electrochemical characteristics suggest that the nanosized LNMO particles are promising for use in high-power lithium-ion batteries.

## Acknowledgements

We gratefully acknowledge the Tarbiat Modares University Research Council for supporting this work (MFM) and Nanotech Energy, Inc (RBK).

## Notes and references

†: Chemistry & Chemical Engineering Research Center of Iran.

‡: Department of Chemistry, Tarbiat Modares University, Tehran, Iran

||: Faculty of basic science, Shahed University, Tehran, Iran

⊖: Department of Chemistry, Faculty of Science, Cairo University, Giza 12613, Egypt.

§: Department of Chemistry and Biochemistry and California NanoSystems Institute, University of California, Los Angeles (UCLA), Los Angeles, CA 90095, USA.

Electronic Supplementary Information (ESI) available: [details of any supplementary information available should be included here]. See DOI: 10.1039/b000000x/

1. M. Armand and J. M. Tarascon, *Nature*, 2008, 451, 652-657.
2. X. Ma, B. Kang and G. Ceder, *J. Electrochem. Soc.*, 2010, 157, A925-A931.
3. H. Xia, Y. S. Meng, L. Lu and G. Ceder, *J. Electrochem. Soc.*, 2007, 154, A737-A743.
4. T. Ohzuku, S. Takeda and M. Iwanaga, *J. Power Sources*, 1999, 81-82, 90-94.
5. T. Ohzuku, K. Ariyoshi, S. Takeda and Y. Sakai, *Electrochim. Acta*, 2001, 46, 2327-2336.
6. H. C. Wang and C. H. Lu, *J. Power Sources*, 2003, 119-121, 738-742.
7. Y. Shin and A. Manthiram, *Electrochim. Acta*, 2003, 48, 3583-3592.

8. Y. Terada, K. Yasaka, F. Nishikawa, T. Konishi, M. Yoshio and I. Nakai, *J. Solid State Chem.*, 2001, 156, 286-291.
9. W. S. Yoon, C. P. Grey, M. Balasubramanian, X. Q. Yang and J. McBreen, *Chem. Mater.*, 2003, 15, 3161-3169.
10. C. S. Johnson, J. S. Kim, A. J. Kropf, A. J. Kahaian, J. T. Vaughey, L. M. L. Fransson, K. Edström and M. M. Thackeray, *Chem. Mater.*, 2003, 15, 2313-2322.
11. M. Kunduraci and R. T. S. U. o. N. J.-N. Brunswick, *High power 4.7 V nanostructured spinel lithium manganese nickel oxide lithium-ion battery cathode materials*, Rutgers The State University of New Jersey - New Brunswick, 2007.
12. Y. Yao, H. Liu, G. Li, H. Peng and K. Chen, *Mater. Chem. Phys.*, 2014, 143, 867-872.
13. X. Zhu, X. Li, Y. Zhu, S. Jin, Y. Wang and Y. Qian, *Electrochim. Acta*, 2014, 121, 253-257.
14. J. Yang, X. Han, X. Zhang, F. Cheng and J. Chen, *Nano Res.*, 2013, 6, 679-687.
15. J. Yang, X. Zhang, Z. Zhu, F. Cheng and J. Chen, *J. Electroanal. Chem.*, 2013, 688, 113-117.
16. X. Zhang, F. Cheng, J. Yang and J. Chen, *Nano Lett.*, 2013, 13, 2822-2825.
17. G. Derrien, J. Hassoun, S. Panero and B. Scrosati, *Adv. Mater.*, 2007, 19, 2336-2340.
18. J. Hassoun, S. Panero, P. Reale and B. Scrosati, *Adv. Mater.*, 2009, 21, 4807-4810.
19. J. Hassoun, P. Reale, S. Panero and B. Scrosati, *Isr. J. Chem.*, 2008, 48, 229-234.
20. R. Verrelli, J. Hassoun, A. Farkas, T. Jacob and B. Scrosati, *J. Mater. Chem. A*, 2013, 1, 15329-15333.
21. G. A. Elia, F. Nobili, R. Tossici, R. Marassi, A. Savoini, S. Panero and J. Hassoun, *J. Power Sources*, 2015, 275, 227-233.
22. L. Lombardo, M. A. Navarra, S. Panero, L. A. Medina, A. Matic and J. Hassoun, *J. Power Sources*, 2014, 245, 232-235.
23. Y. Idemoto, H. Narai and N. Koura, *J. Power Sources*, 2003, 119-121, 125-129.
24. J. C. Arrebola, A. Caballero, M. Cruz, L. Hernán, J. Morales and E. R. Castellón, *Adv. Funct. Mater.*, 2006, 16, 1904-1912.
25. M. Kunduraci and G. G. Amatucci, *Electrochim. Acta*, 2008, 53, 4193-4199.
26. J. Gao, J. Li, C. Jiang and C. Wan, *J. Electrochem. Soc.*, 2010, 157, A899-A902.
27. X. Zhang, J. Liu, H. Yu, G. Yang, J. Wang, Z. Yu, H. Xie and R. Wang, *Electrochim. Acta*, 2010, 55, 2414-2417.
28. M. G. Lazarraga, L. Pascual, H. Gadjov, D. Kovacheva, K. Petrov, J. M. Amarilla, R. M. Rojas, M. A. Martín-Luengo and J. M. Rojo, *J. Mater. Chem.*, 2004, 14, 1640-1647.
29. S. H. Oh, K. Y. Chung, S. H. Jeon, C. S. Kim, W. I. Cho and B. W. Cho, *J. Alloys Compd.*, 2009, 469, 244-250.
30. L. H. Chi, N. N. Dinh, S. Brutti and B. Scrosati, *Electrochim. Acta*, 2010, 55, 5110-5116.
31. Y. Gogotsi, *ACS Nano*, 2014, 8, 5369-5371.
32. M. A. Kiani, M. F. Mousavi and S. Ghasemi, *J. Power Sources*, 2010, 195, 5794-5800.
33. M. A. Kiani, M. F. Mousavi and M. S. Rahmanifar, *Int. J. Electrochem. Sci.*, 2011, 6, 2581-2595.
34. K. Ghanbari, M. F. Mousavi and M. Shamsipur, *Electrochim. Acta*, 2006, 52, 1514-1522.
35. A. Pendashteh, M. F. Mousavi, M. A. Kiani, S. H. Kazemi and M. S. Rahmanifar, *J. Iran. Chem. Soc.*, 2012, 9, 389-395.
36. H. R. Ghenaatian, M. F. Mousavi, S. H. Kazemi and M. Shamsipur, *Synth. Met.*, 2009, 159, 1717-1722.
37. H. R. Ghenaatian, M. F. Mousavi and M. S. Rahmanifar, *Synth. Met.*, 2011, 161, 2017-2023.
38. A. Pendashteh, M. F. Mousavi and M. S. Rahmanifar, *Electrochim. Acta*, 2013, 88, 347-357.
39. H. R. Ghenaatian, M. F. Mousavi and M. S. Rahmanifar, *Electrochim. Acta*, 2012, 78, 212-222.
40. A. Pendashteh, M. S. Rahmanifar, R. B. Kaner and M. F. Mousavi, *Chem. Commun.*, 2014, 50, 1972-1975.
41. A. Pendashteh, M. S. Rahmanifar and M. F. Mousavi, *Ultrason. Sonochem.*, 2014, 21, 643-652.
42. M. Y. Elahi, M. F. Mousavi and S. Ghasemi, *Electrochimica Acta*, 2008, 54, 490-498.
43. K. Ghanbari, S. Z. Bathaie and M. F. Mousavi, *Biosens. Bioelectron.*, 2008, 23, 1825-1831.
44. M. Yousef Elahi, S. Z. Bathaie, S. H. Kazemi and M. F. Mousavi, *Anal. Biochem.*, 2011, 411, 176-184.
45. A. Mehdinia, S. H. Kazemi, S. Z. Bathaie, A. Alizadeh, M. Shamsipur and M. F. Mousavi, *J. Pharm. Biomed. Anal.*, 2009, 49, 587-593.
46. A. Mehdinia, M. F. Mousavi and M. Shamsipur, *J. Chromatogr. A*, 2006, 1134, 24-31.
47. D. Li, A. Ito, K. Kobayakawa, H. Noguchi and Y. Sato, *Electrochim. Acta*, 2007, 52, 1919-1924.
48. R. Alcántara, M. Jaraba, P. Lavela and J. L. Tirado, *Electrochim. Acta*, 2002, 47, 1829-1835.
49. Q. Zhong, A. Bonakdarpour, M. Zhang, Y. Gao and J. R. Dahn, *J. Electrochem. Soc.*, 1997, 144, 205-213.
50. S. Park and Y. Sun, *Electrochim. Acta*, 2004, 50, 434-439.
51. K. Ariyoshi, Y. Iwakoshi, N. Nakayama and T. Ohzuku, *J. Electrochem. Soc.*, 2004, 151, A296-A303.
52. J. H. Kim, S. T. Myung, C. S. Yoon, S. G. Kang and Y. K. Sun, *Chem. Mater.*, 2004, 16, 906-914.
53. X. Zhang, H. Zheng, V. Battaglia and R. L. Axelbaum, *Proc. Combust. Inst.*, 2011, 33, 1867-1874.
54. Q. Zhong, A. Bonakdarpour, M. Zhang, Y. Gao and J. R. Dahn, *J. Electrochem. Soc.*, 1997, 144, 205-213.
55. A. Van Der Ven, C. Marianetti, D. Morgan and G. Ceder, *Solid State Ionics*, 2000, 135, 21-32.
56. H. Jiang, Y. Fu, Y. Hu, C. Yan, L. Zhang, P. S. Lee and C. Li, *Small*, 2014, 10, 1096-1100.
57. J. Liu and A. Manthiram, *J. Electrochem. Soc.*, 2009, 156, A66-A72.
58. K. M. Shaju and P. G. Bruce, *Dalton Trans.*, 2008, 5471-5475.
59. N. Zhang, T. Yang, Y. Lang and K. Sun, *J. Alloys Compd.*, 2011, 509, 3783-3786.
60. Y. Ding, P. Zhang and D. Gao, *J. Alloys Compd.*, 2008, 456, 344-347.
61. K. A. Striebel, A. Rougier, C. R. Horne, R. P. Reade and E. J. Cairns, *J. Electrochem. Soc.*, 1999, 146, 4339-4347.
62. Y. S. Lee, N. Kumada and M. Yoshio, *J. Power Sources*, 2001, 96, 376-384.
63. K. Takahashi, M. Saitoh, M. Sano, M. Fujita and K. Kifune, *J. Electrochem. Soc.*, 2004, 151, A173-A177.
64. D. Linden and T. B. Reddy, *Handbook of batteries*, McGraw-Hill Companies, Inc., New York, Third edn., 2002.
65. K. S. Suslick, S. B. Choe, A. A. Cichowlas and M. W. Grinstaff, *Nature*, 1991, 353, 414-416.
66. D. Chaumont, A. Craievich and J. Zarzycki, *J. Non-Cryst. Solids*, 1992, 147-148, 41-46.
67. M. Kunduraci, J. F. Al-Sharab and G. G. Amatucci, *Chem. Mater.*, 2006, 18, 3585-3592.
68. A. S. Aricò, P. Bruce, B. Scrosati, J. M. Tarascon and W. Van Schalkwijk, *Nat. Mater.*, 2005, 4, 366-377.
69. E. Lee and K. A. Persson, *Nanotechnology*, 2013, 24, 424007.